

MOLECULAR OUTFLOWS: EXPLOSIVE VERSUS PROTOSTELLAR

LUIS A. ZAPATA¹, JOHANNES SCHMID-BURGK²,
LUIS F. RODRÍGUEZ¹, AINA PALAU¹, AND LAURENT LOINARD¹
ApJ

ABSTRACT

With the recent recognition of a second, distinctive class of molecular outflows, namely the explosive ones not directly connected to the accretion-ejection process in the star formation, a juxtaposition of the morphological and kinematic properties of both classes is warranted. By applying the same method used in Zapata et al. (2009), and using ¹²CO(J=2-1) archival data from the Submillimeter Array (SMA), we contrast two well known explosive objects, Orion KL and DR21, to HH211 and DG Tau B, two flows representative of classical low-mass protostellar outflows. At the moment there are only two well established cases of explosive outflows, but with the full availability of ALMA we expect that more examples will be found in the near future. Main results are the largely different spatial distributions of the explosive flows, consisting of numerous narrow straight filament-like ejections with different orientations and in almost an isotropic configuration, the red with respect to the blueshifted components of the flows (maximally separated in protostellar, largely overlapping in explosive outflows), the very well-defined Hubble flow-like increase of velocity with distance from the origin in the explosive filaments versus the mostly non-organized CO velocity field in protostellar objects, and huge inequalities in mass, momentum and energy of the two classes, at least for the case of low-mass flows. Finally, all the molecular filaments in the explosive outflows point back to approximately a central position (*i.e.* the place where its “exciting source” was located), contrary to the bulk of the molecular material within the protostellar outflows.

Subject headings: stars: protostars, ISM: jets and outflows, individual (Orion KL, DR21, HH 211, DG Tau B, IRAS 18162-2048-NW, IRAS 18360-0537)

1. INTRODUCTION

Since their discovery, the explosive outflows have formed part of a new class of molecular outflows related with star forming regions (Zapata et al. 2009). At this moment, there seem to exist two kinds of molecular outflows related with star forming regions (Frank et al. 2014; Bally 2016). One kind are the *protostellar* molecular outflows energized by a star in its process of formation (see for a review, Arce et al. 2007), and the other kind are the *explosive* molecular outflows, probably associated with the disruption of a non-hierarchical massive and young stellar system (triggered by the possible merger of young massive stars), or with a protostellar collision (*e.g.*, Zapata et al. 2009; Bally et al. 2011; Zapata et al. 2013a; Rivilla et al. 2014; Bally 2016; Bally et al. 2017). Hence, the occurrence of the two types of molecular flows could point to the existence of two totally different physical phenomena (Zapata et al. 2009). In order to distinguish between the two outflow phenomena it is therefore required to study their morphological and kinematic differences.

The general agreement is that the molecular outflows associated with the process of star formation (energized by means of a circumstellar accreting disk) are probably formed by the interaction between the molecular material from the parental cloud and the ionized/neutral collimated jet ejected from the young star, that creates internal jet working surfaces (Masson & Chernin 1993; Raga & Cabrit 1993). This interaction additionally produces bow-shocks, cavities, swept-up shells and jet shocks, see for example the cases of the HH 211, DG Tau B, IRAS 18162-2048-NW and IRAS 18360-

0537 (Froebrich 2005; Palau et al. 2006; Qiu et al. 2012; Fernández-López et al. 2013; Zapata et al. 2015) or the Serpens South outflow (Plunkett et al. 2015). However, there is a large amount of cases where even molecular material is present in form of collimated jets (where the ionized/neutral gas is supposedly located), see for an example the cases of the HH 211 or Serpens South outflows (Palau et al. 2006; Plunkett et al. 2015). The nature of the primary collimated jet is still under debate. At this time, it is hypothesized that such primary jets are driven and collimated by rapidly rotating magnetic fields coupled to the star/disk system (Pudritz et al. 2007; Frank et al. 2014; Arce et al. 2007).

On the other hand are the explosive outflows, recently reported and discussed in the literature (*e.g.*, Zapata et al. 2009, 2013a; Bally et al. 2011; Youngblood et al. 2016; Bally 2016). The explosive flows seem to be impulsive, and created possibly by an energetic single and brief event (Bally & Zinnecker 2005). These flows consist of dozens of expansive CO filaments, [FeII] fingers, and H₂ wakes pointing back approximately to a central position, reminiscent of an explosive event, see the cases of DR21 or Orion KL (Allen & Burton 1993; Zapata et al. 2009, 2013a; Youngblood et al. 2016). The expansive CO filaments are nearly isotropic on the sky and present well defined Hubble velocity laws, that is the radial velocities increase with the projected distances (see Figure 2 of Zapata et al. 2009, 2013a; Bally et al. 2017). In the case of Orion KL, the dynamical ages of most CO filaments are close to 500 yrs, the age of the disruption of a non-hierarchical massive and young stellar system (Gómez et al. 2005; Zapata et al. 2009) which is the event that probably originated the outflow. As the explosive flow in Orion KL has no longer an “exciting” source it should not last for a long time as compared to the long-lives of the protostellar outflows with dynamical timescales of about

¹ Instituto de Radioastronomía y Astrofísica, UNAM, Apdo. Postal 3-72 (Xangari), 58089 Morelia, Michoacán, México

² Max-Planck-Institut für Radioastronomie, Auf dem Hügel 69, 53121, Bonn, Germany

10^{4-5} years (Frank et al. 2014; Bally 2016).

The precise nature of the explosive outflows is still not well understood but it is speculated that it might be related to the disintegration of young stellar systems –as mentioned above and revealed in the case of Orion KL (Bally & Zinnecker 2005; Zapata et al. 2009; Bally et al. 2011, 2017). Bally et al. (2015) proposed that the optical bullets in Orion KL are probably dense fragments of interacting circumstellar disks that were torn apart in a stellar encounter and launched into the surrounding cloud. The high tangential velocities of the optical bullets (~ 300 km s $^{-1}$; Doi et al. 2002) were inherited from the very inner Keplerian velocities of the disks. This implies that the H $_2$ wakes are probably warm gas trails of a large numbers of expelled chunks or bullets observed at a wide range of wavelengths. As to the CO filaments, their nature is unclear, they could also be small chunks of disks with different velocities, or warm gas trails.

In this study, we present Submillimeter Array $^{12}\text{CO}(J=2-1)$ observations of the two classical molecular outflows HH211 and DG Tau B excited by stars in their process of formation, and of two recently recognized explosive outflows (Orion KL and DR21) associated with massive star forming regions. The main reason for this comparison with the low-mass stars is the large outflow multiplicity observed in the high-mass protostars, see for example the cases of IRAS 05358+3543 (Beuther et al. 2002), G240.31+0.07 (Qiu et al. 2009), and IRAS 17233-3606 (Leurini et al. 2009; Klaassen et al. 2015). This high outflow multiplicity difficulties the identification of any physical and kinematical difference between both kinds of flows. The new analysis conducted in these CO observations allow us to compare for the first time, the morphological and kinematic properties of both classes of molecular outflows.

2. ARCHIVAL SMA OBSERVATIONS

2.1. HH211

The millimeter $^{12}\text{CO}(J=2-1)$ data were collected on 2008 November 16 with the Submillimeter Array³, when the array was in its compact configuration. The independent baselines in this configuration ranged in projected length from 6 to 60 k λ . The phase reference center of the observations was situated at the position $\alpha_{J2000.0} = 04^{\text{h}}27^{\text{m}}02^{\text{s}}.66$, $\delta_{J2000.0} = +26^{\circ}05'30''.4$, located toward the southeastern terminal shock of the HH211 jet. This allowed to better trace the molecular component from this side of the flow. The SMA primary beam is approximately $55''$ at 230 GHz. During these millimeter observations the zenith opacity was reasonable, ranging from 0.1 to 0.3, and resulting thus in stable phases during the whole track. The digital correlator was set to have 24 spectral "chunks" of 104 MHz and 256 channels each. This spectral resolution yielded a velocity resolution of about 0.5 km s $^{-1}$ per channel, however, we smoothed it to ~ 1.0 km s $^{-1}$. The quasars 3C84, and 3C111 were used as bandpass and gain calibrators, while one of the Saturn's moon, Titan, was used as flux calibrator. The uncertainty in the flux scale is estimated to be between 15% and 20%, based on the SMA monitoring of quasars. The rest frequency of the $^{12}\text{CO}(J=2-1)$ is 230.5379944 GHz and was detected in the upper sideband of the SMA observations.

The ^{12}CO data were calibrated using the IDL superset

MIR adapted for the SMA⁴. The calibrated data were imaged and analyzed in the standard manner using the MIRIAD (Sault et al. 1995) and KARMA (Gooch 1996) softwares⁵. A $^{12}\text{CO}(J=2-1)$ velocity cube was obtained setting the ROBUST parameter of the task INVERT to +2 to obtain a better sensitivity while losing some angular resolution. The contribution from the continuum was removed. The resulting r.m.s. noise for the velocity data cube was about 30 mJy beam $^{-1}$ per channel, at an angular resolution of $3''.0 \times 2''.4$ with a P.A. = -56.7° .

2.2. DG Tau B

The millimeter $^{12}\text{CO}(J=2-1)$ data were collected on 2011 November with the Submillimeter Array, when the array was in its compact configuration. The independent baselines in these configurations ranged in projected length from 10 to 140 k λ . The phase center is located at the position $\alpha_{J2000.0} = 04^{\text{h}}27^{\text{m}}02^{\text{s}}.66$, $\delta_{J2000.0} = +26^{\circ}05'30''.4$. The SMA digital correlator was set to have 48 spectral "chunks" of 104 MHz and 128 channels each. This spectral resolution yielded a velocity resolution of about 1 km s $^{-1}$ per channel, however, the spectral "chunk" where the CO is located allowed 512 channels of resolution providing a better velocity resolution (~ 0.5 km s $^{-1}$). The planet Uranus was used to obtain the absolute scale for the flux density calibration. The gain calibrators were the quasars 3C 111 and 3C 84, while 3C 279 was used for bandpass calibration.

The CO data were calibrated and imaged using MIR, KARMA, and MIRIAD. A CO velocity cube was obtained setting the ROBUST parameter of the task INVERT to +2 to obtain a better sensitivity losing some angular resolution. The contribution from the continuum was removed. The resulting r.m.s. noise for the cube line was about 90 mJy beam $^{-1}$ per channel, at an angular resolution of $3''.28 \times 2''.9$ with a P.A. = -64.5° .

2.3. Orion KL

The $^{12}\text{CO}(J=2-1)$ data were collected on 2007 January and 2009 January with the Submillimeter Array, when the array was in its compact and subcompact configurations. The independent baselines in these configurations ranged in projected length from 6 to 58 k λ . A mosaic with half-power point spacing between field centers covered the entire BN/KL outflow, see Zapata et al. (2009). During these millimeter observations the zenith opacity was also reasonable, ranging from 0.1 to 0.3. The SMA digital correlator was set to have 24 spectral windows ("chunks") of 104 MHz each, with 256 channels distributed over each spectral window, thus providing a spectral resolution of 0.40 MHz (1.05 km s $^{-1}$) per channel. We smoothed the spectral resolution to 5 km s $^{-1}$. The planet Uranus, and Titan were used to obtain the absolute scale for the flux density calibration. The gain calibrators were the quasars J0530+135, J0607-085 and J0541-056. The CO line was detected in the in the upper sideband of the SMA observations.

The CO data were calibrated and imaged using MIR, KARMA, and MIRIAD. A CO velocity cube also was obtained setting the ROBUST parameter of the task INVERT to 0 to obtain an optimal compromise between sensitivity and

³ The Submillimeter Array (SMA) is a joint project between the Smithsonian Astrophysical Observatory and the Academia Sinica Institute of Astronomy and Astrophysics, and is funded by the Smithsonian Institution and the Academia Sinica.

⁴ The MIR-IDL cookbook by C. Qi can be found at <http://cfa-www.harvard.edu/cqi/mircook.html>

⁵ The raw data can be obtained from: <http://www.cfa.harvard.edu/>

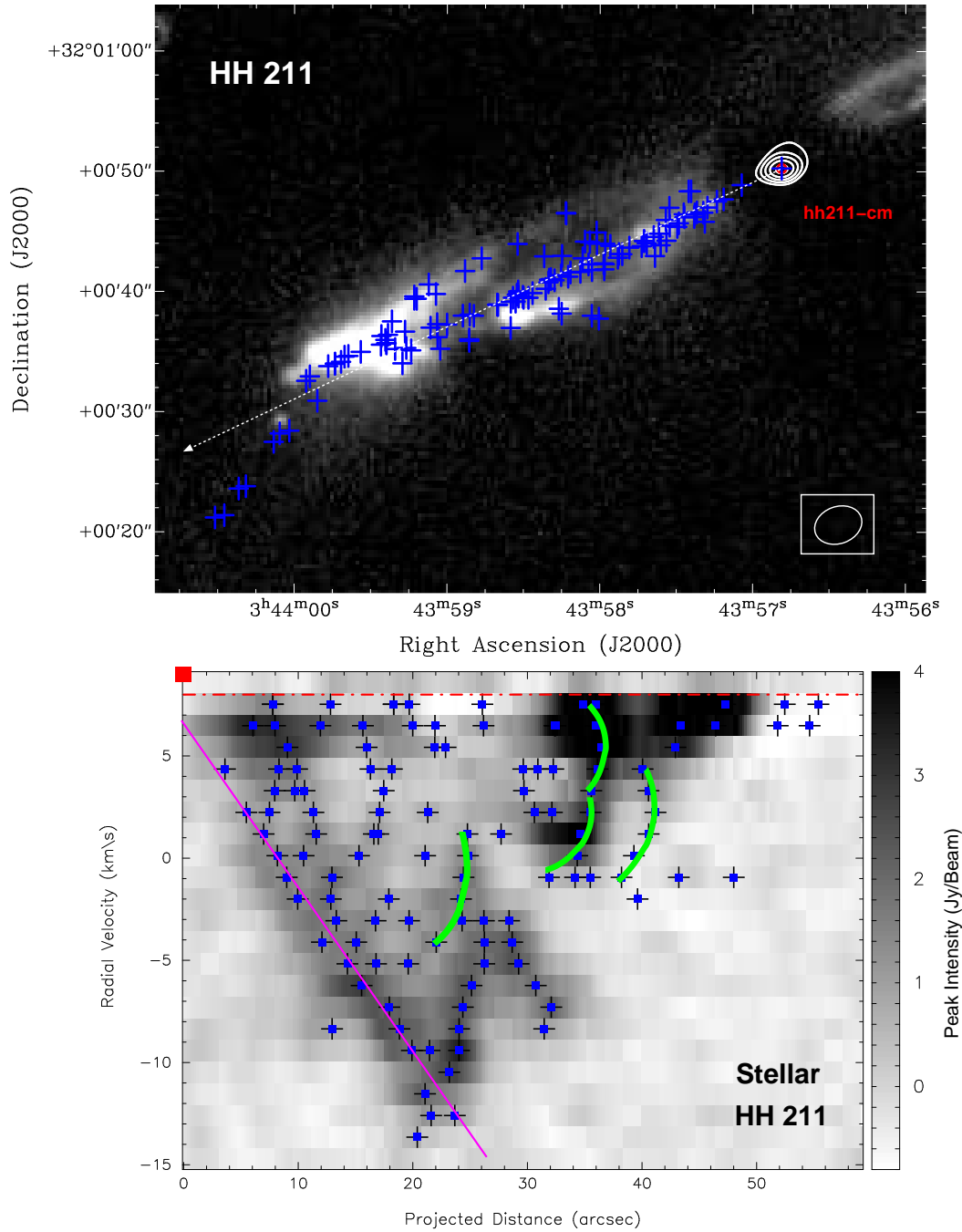


FIG. 1.— *Upper:* H_2 infrared line ($2.122 \mu\text{m}$) image of the blueshifted side of the molecular outflow HH 211 (McCaughrean et al. 1994), overlaid with the SMA positions of the $^{12}\text{CO}(J=2-1)$ blueshifted compact condensations revealed in the spectral data cube (blue crosses), and the 3.3 cm continuum emission mapped by the VLA (white contours, Rodríguez et al. 2014). The red circle and blue cross (on top of the white contours) mark the peak position of the 3.3 cm source. The white contours are in percent of the peak emission starting from 40% to 90%, in steps of 10%. The intensity peak emission is $0.18 \text{ mJy Beam}^{-1}$. The half-power contour of the synthesized beam of the 3.3 cm image is shown in the bottom right corner. The dashed arrow marks the position of the cut shown below and its orientation toward positive values. *Lower:* Position velocity diagram of the blueshifted $^{12}\text{CO}(J=2-1)$ emission from the HH 211 outflow, overlaid with the SMA positions of the blueshifted compact condensations revealed in each channel of the spectral data cube (blue crosses). The position velocity diagram is made along the blueshifted jet axis at a P.A. = 115° , see upper panel. peaks revealed in the position-velocity diagram. The red dashed line marks the systemic velocity of the cloud. The emission inside of this range cannot be well sampled by the SMA. The red square indicates the position of the continuum 3.3 cm source and its systemic velocity ($\sim 9.0 \text{ km s}^{-1}$; Palau et al. 2006). The pink line marks the tentative Hubble velocity law observed in the protostellar outflow. The green curve trace the bow-shocks revealed across the flow.

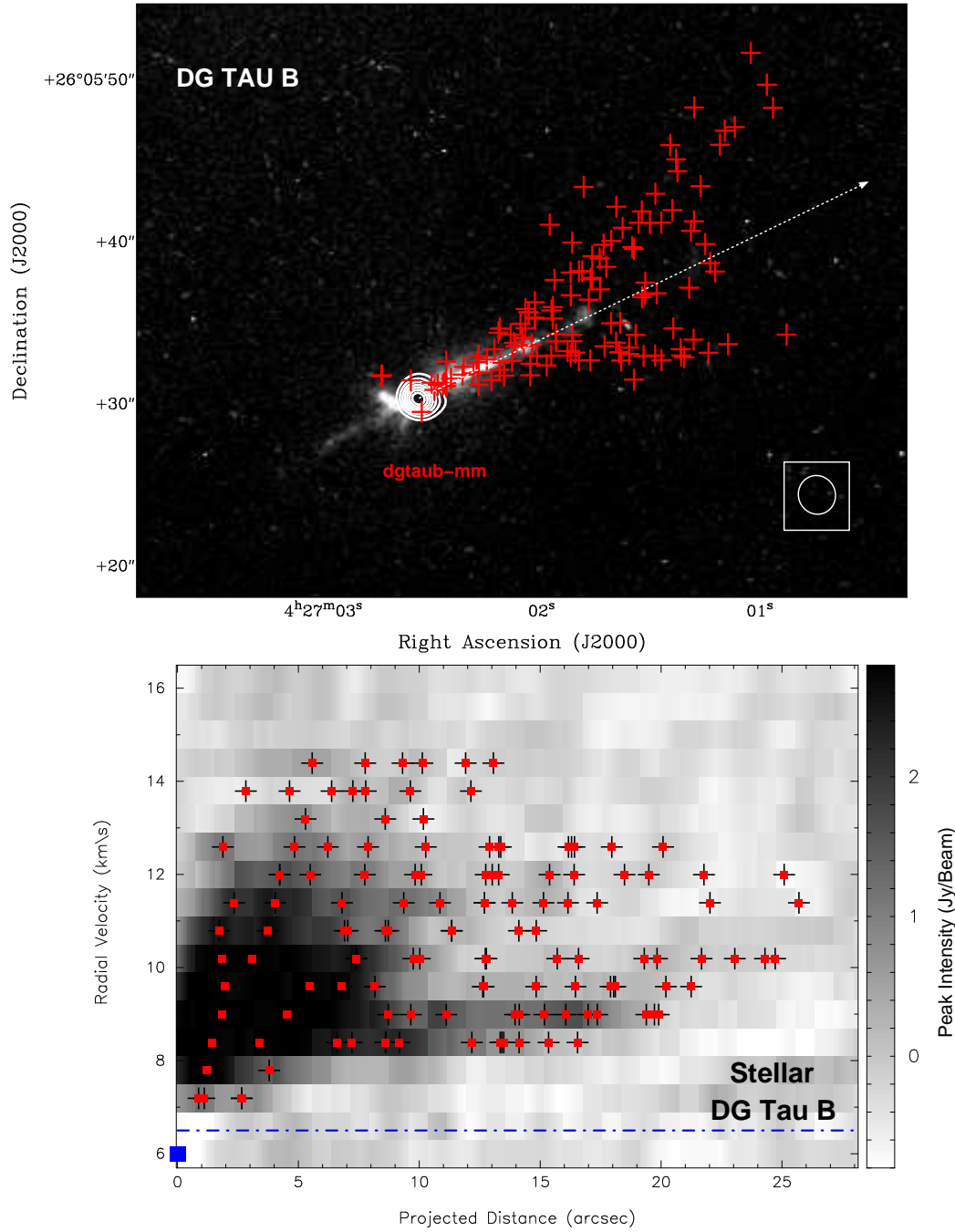


FIG. 2.— *Upper*: HST-WFPC optical image (F675w) of the molecular outflow DG Tau B, overlaid with the SMA positions of the $^{12}\text{CO}(J=2-1)$ redshifted compact condensations revealed in the spectral data cube (red crosses), and the 1.3 mm continuum emission mapped with the SMA (white contours, Zapata et al. 2015). The white contours are in percent of the peak emission starting from 30% to 90%, in steps of 10%. The intensity peak emission is $0.31 \text{ Jy Beam}^{-1}$. The half-power contour of the synthesized beam of the 1.3 mm image is shown in the bottom right corner. The dashed arrow marks the position of the cut shown below and its orientation toward the positive values. *Lower*: Position-velocity diagram of the redshifted $^{12}\text{CO}(J=2-1)$ emission from the DG Tau B outflow, overlaid with the SMA positions of the redshifted emission peaks in each channel revealed in the spectral data cube (red crosses). The PV diagram is made along the red-shifted jet axis at a P.A. = 296° , see Figure 3. the systemic velocity of the cloud. The emission inside of this range cannot be sampled well by the SMA. The blue square indicates the position of the continuum 1.3 cm source and its systemic velocity ($\sim 6.5 \text{ km s}^{-1}$; Zapata et al. 2015).

angular resolution. The contribution from the continuum was also removed. The resulting r.m.s. noise for the cube line was about $200 \text{ mJy beam}^{-1}$ per channel, at an angular resolution of $3''.28 \times 3''.12$ with a P.A. = -14.0° .

2.4. DR21

The $^{12}\text{CO}(J=2-1)$ data were collected on 2011 August and 2012 July/August with the Submillimeter Array, when the array was in its extended, compact, and subcompact configuration. The independent baselines in these configurations ranged in projected length from 7 to 160 k λ . This observation used the mosaicking mode with half-power point spacing between field centers to cover the entire DR21 flow, see Zapata et al. (2013a). The SMA correlator was set to have 24 spectral “chunks” of 104 MHz and 128 channels each. This spectral resolution yielded a velocity resolution of about 1.05 km s^{-1} . During these millimeter observations the zenith opacity was reasonable, ranging from 0.1 to 0.3, and resulting thus in stable phases during the whole track. The gain calibrators were the emission-line star MWC 349A, and the quasar J2007+404. The planet Uranus was used to obtain the absolute scale for the flux density calibration. The CO line also was detected in the upper sideband of the SMA observations.

The CO data were calibrated and imaged using MIR, KARMA, and MIRIAD. A CO velocity cube was obtained setting the ROBUST parameter of the task INVERT to 0 to obtain an optimal compromise between sensitivity and angular resolution. The contribution from the millimeter continuum was removed. The resulting r.m.s. noise for the cube line was about $100 \text{ mJy beam}^{-1}$, at an angular resolution of $2''.17 \times 1''.89$ with a P.A. = $+74.0^\circ$.

3. RESULTS

In this study we have applied the method used in Zapata et al. (2009) to the spectral data cubes obtained from the SMA archive for the outflows: HH211, DG Tau B, Orion KL, and DR 21. In the cases of Orion KL and DR 21, we only applied this to a few isolated filaments. This method fits 2D gaussians to extract the position and radial velocities of the molecular condensations detected above of 5σ -level above the rms noise of each channel.

In Figures 1, 2, 3, and 4 we show the main results of this study. In these Figures, we present the position of the most prominent CO features revealed in the velocity cubes obtained with the SMA, overlaid with the H_2 and optical images of the two classical protostellar outflows (HH 211 and DG Tau B) and the two explosive ones (Orion KL and DR 21). For simplicity, we have only studied the blue-shifted side of the HH 211, and red-shifted side of the DG Tau B outflow. We argue that both sides of such outflows have a similar gas kinematic behaviour, as revealed in the position velocity diagrams, and velocity cubes of Mitchell et al. (1994); Hirano et al. (2006); Palau et al. (2006); Zapata et al. (2015). However, in the case of DG Tau B it is very clear from the optical and millimeter observations that the outflow is asymmetric, with the north-west side being more prominent, see Figure 2. The latter is the side that we are studying here. Moreover, the object exciting the outflow in DG Tau B is associated with a T Tauri star (Class I/II; Mundt & Fried 1983), while the source of HH 211 is related with a younger Class 0 protostar (Palau et al. 2006). In Figures 1 and 2, we have included continuum compact emission from their exciting sources to clarify their locations. For the explosive outflows case, we have selected only three CO filaments, one in DR21 and two in Orion KL.

These filaments are mostly isolated and so let us better trace their kinematics, see Figures 3 and 4. All filaments present a similar gas kinematical behaviour, *i.e.* well defined Hubble velocity laws, see the position-velocity CO diagrams in Zapata et al. (2009, 2013a). Hence, these filaments represent well the kinematics of the explosive outflows from a general point of view.

In Figure 1, in the upper panel, we show the resulting SMA image for the blue-shifted side of the protostellar outflow HH 211 overlaid with the H_2 emission obtained from McCaughrean et al. (1994). The blue crosses mark the position of the CO condensations at different radial velocities extracted from the data cube. The blue crosses delineate very well the infrared H_2 structure and are in good agreement with the morphology revealed in the moment zero CO maps presented in Tappe et al. (2012). Our image even reveals the outflow deflection occurring on the southeast far tip of this blue-shifted component, and bow-shock structures across the outflow. Furthermore, the molecular outflow appears to have a double component, one component in the middle that is collimated (the molecular jet) and another one more extended surrounding the molecular jet. This double molecular structure has already been noted in older interferometric observations (Gueth & Guilloteau 1999) and explained in terms of a jet-driven flow. In this image, we have also overlaid the centimeter emission from the exciting object of the HH 211 outflow as mentioned before, see Rodríguez et al. (2014). The centimeter source traces well the origin of the blue-shifted CO molecular emission. In the lower panel of Figure 1, we present the Position-Velocity Diagram (PVD) from the blue-shifted side of the flow overlaid with the positions of the CO molecular condensations presented in the upper panel of Figure 1. The PVD diagram was made along the outflow axis (115°). In this PVD, we have also marked the position of the exciting source of HH 211 as mentioned above.

In Figure 2, in the upper panel, we show the resulting SMA image for the red-shifted side of the protostellar outflow DG Tau B overlaid with an optical HST image obtained from the HST Legacy Archive⁶. The crosses, as in the HH 211 outflow, trace the position of the CO condensations at different radial velocities extracted from the data cube, but in this case tracing red-shifted emission. As one can see the red crosses trace very well the entrained gas in the vicinities of the optical jet. The morphology of the red crosses is very similar to that obtained in the moment zero map of CO presented in Zapata et al. (2015). We have also overlaid the millimeter continuum emission from DG Tau B obtained from Zapata et al. (2015). This emission traces the circumstellar inner disk that surrounds the exciting source of the outflow. A PVD was also extracted from the CO data cube with a Position Angle (P.A.) similar to that of the outflow axis (296°). This PVD is presented in the lower panel of Figure 2. In this PVD, we have also marked the position of the exciting source of DG Tau B.

In Figure 3, in the upper panel, we present the image obtained by Zapata et al. (2009) from the explosive outflow in Orion KL, used here only as a reference, and a zoom into a relatively isolated zone with only a small number of filaments. In this zone we have selected two filaments with a similar P.A. equal to 54° named Orion Filament (OF) 1 and 2. OF1 is somehow more extended than OF2, suggesting that they may have different angles with respect to the plane of sky. These two filaments are composed of CO condensations at different

⁶ <https://hla.stsci.edu/hlaview.html>

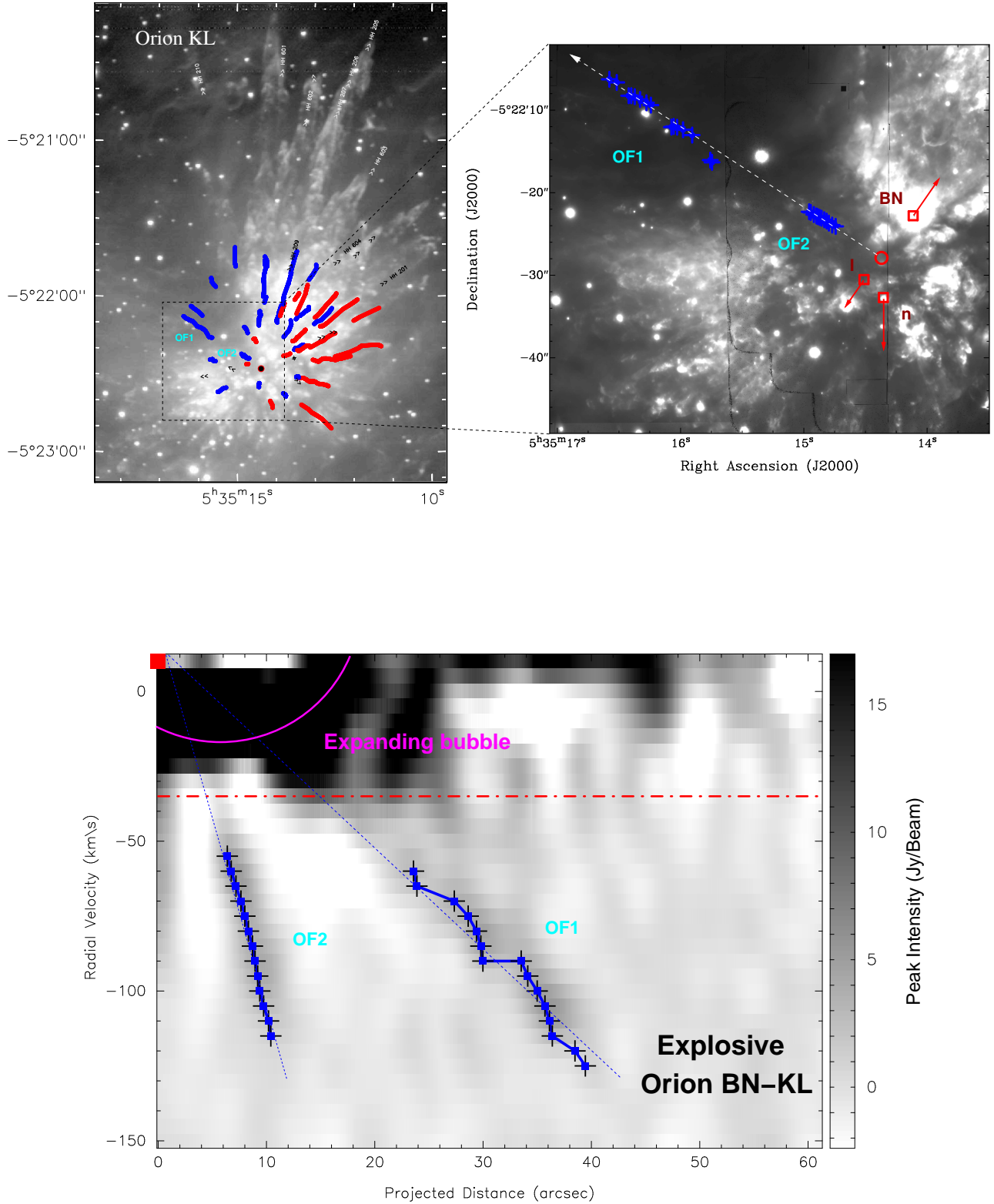


FIG. 3.— *Upper Left Panel:* H₂ infrared line image from the molecular outflow in Orion KL (Bally et al. 2011, 2015), overlaid with the SMA positions of the ¹²CO(J=2-1) red- and blueshifted compact condensations revealed in the spectral data cube (red and blue “filaments”) and reported in Zapata et al. (2009). All filaments point toward the same central position marked here with a red/black circle. Optical objects moving away from this center are shown as small arrows that indicate the direction of their motion (Doi et al. 2002; O’Dell et al. 2008). *Right Panel:* a zoom into the center of the outflow overlaid with the positions of the runaway sources BN, Source I, and n, and the blueshifted “filaments” OF1 and OF2. The red arrows mark the the direction of the proper motion of the three runaway objects (Rodríguez et al. 2005; Gómez et al. 2005, 2008). The red circle represents the zone from where the three objects were ejected 500 years ago (Gómez et al. 2005). The dashed arrow marks the position of the cut shown in the lower-panel and its orientation toward the positive values. *Lower* Position-velocity diagram of the two blueshifted ¹²CO(J=2-1) “filaments” called OF1 and OF2 (shown in the upper panel), overlaid with the positions of the compact condensations revealed in the spectral data cube (blue crosses), see Zapata et al. (2009). The PV diagram is made along a P.A. = 54°, see the upper panel. The red dashed line marks the position of the starting velocity range where the systemic velocity of the cloud is located. The emission inside of this range cannot be well sampled by the SMA. The red square indicates the position of the origin of the explosive outflow and its systemic velocity (~9.0 km s⁻¹; Zapata et al. 2009; Rodríguez et al. 2009). The truncated magenta circle shows part of the expanding molecular bubble reported in Zapata et al. (2011). The blue dashed lines trace the orientation of each filament.

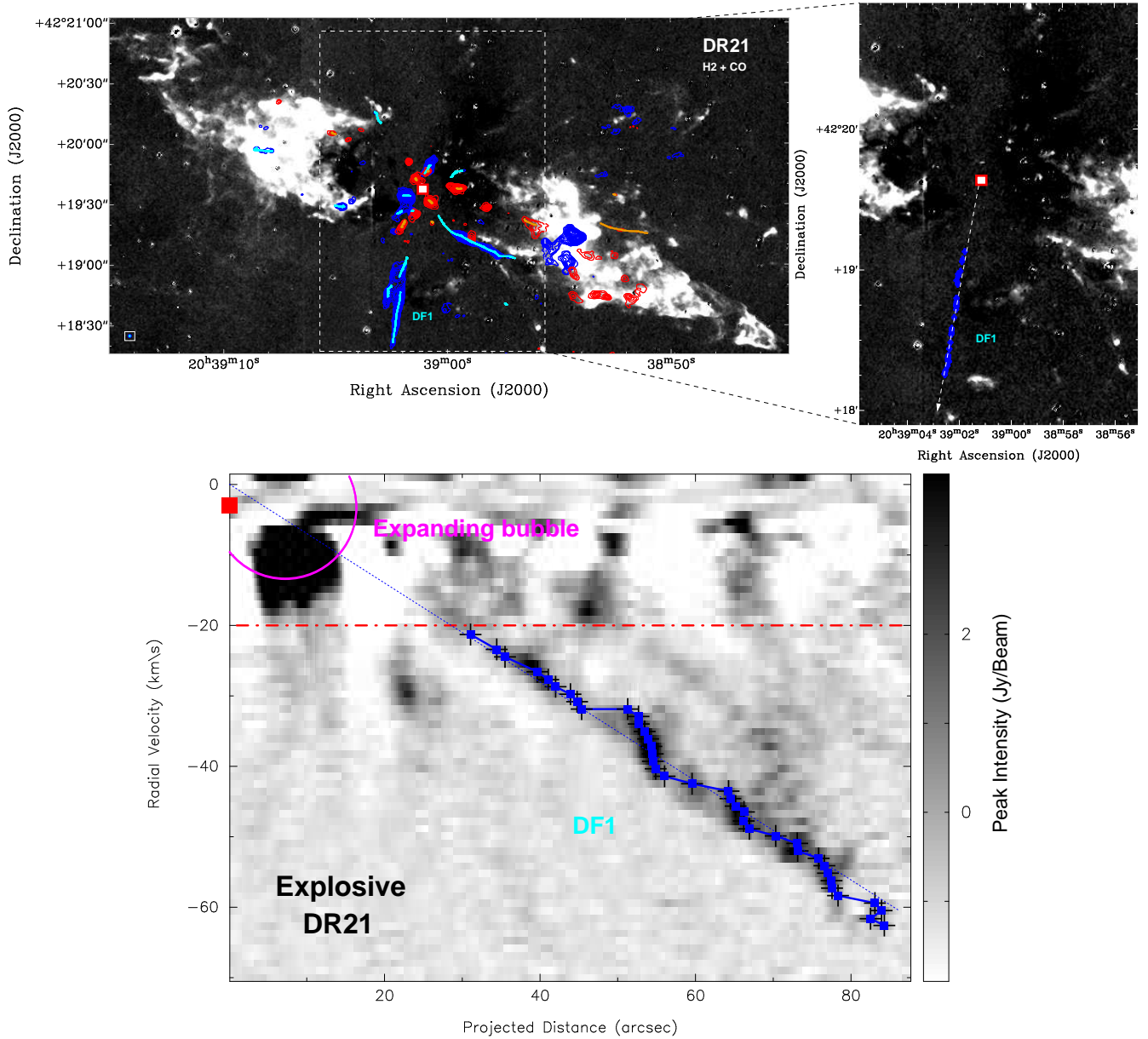


FIG. 4.— *Upper*: Left Panel: H₂ infrared line image from the molecular outflow in DR21 (Davis et al. 2007), overlaid with the SMA positions of the ¹²CO(J=2-1) red- and blueshifted compact condensations revealed in the spectral data cube (red and blue “filaments”), and the moment zero map of the CO emission, reported in Zapata et al. (2013a). The blue and red contours trace the ¹²CO(J=2-1) molecular emission reported in Zapata et al. (2013a). The contour values are the same as Figure 1 presented in Zapata et al. (2013a). All filaments point toward the same central position marked here with a red box. Right Panel: a zoom into the center of the outflow overlaid with the position of the center of the explosive outflow (red box), and the blueshifted “filament” DF1. The dashed arrow marks the position of the cut shown in the lower panel and its orientation toward the positive values. *Lower*: Position-velocity diagram of the blueshifted ¹²CO(J=2-1) “filament” called DF1 (shown in the upper-panel), overlaid with the positions of the compact condensations revealed in the spectral data cube (blue crosses), see Zapata et al. (2013a). The PV diagram is made along a P.A. = 174°, see upper panel. The position of the condensations (shown here as black crosses with a blue square at the center) are in very good agreement with the CO emission peaks revealed in the position-velocity diagram. The red dashed line marks the position of the starting velocity range where the systemic velocity of the cloud is located. The emission inside of this range cannot be well sampled by the SMA. The red square indicates the position of the origin of the explosive outflow and the systemic velocity (-3.0 km s^{-1} ; Zapata et al. 2013a). The truncated magenta circle shows part of the expanding molecular bubble reported in Zapata et al. (2017), in prep. The blue dashed lines trace the orientation of the filament.

TABLE 1
PHYSICAL PARAMETERS OF THE EXPLOSIVE AND PROTOSTELLAR OUTFLOWS

Name	Mass [M_{\odot}]	Mean Velocity [km s^{-1}]	Momentum [$M_{\odot} \text{ km s}^{-1}$]	Energy [10^{45} erg]	Dynamical Age [years]	Mechanical Luminosity [L_{\odot}]
<i>Explosive Outflows (One single filament)</i>						
Orion KL ^a	≥ 0.12	70	8.4	5.9	~ 500	~ 93
DR21 ^b	≥ 0.51	40	20.5	8.2	$\sim 10^4$	~ 6.5
<i>Protostellar Low-mass Outflows</i>						
HH 211 ^c (blue lobe)	≥ 0.0015	20	0.03	0.006	3×10^3	0.01
DG Tau B ^f	≥ 0.0025	20	0.05	0.01	700	0.1
<i>Protostellar Massive Outflows</i>						
IRAS 18162–2048-NW ^c	0.74	12.1	9	1.5	5×10^3	2
IRAS 18360–0537 ^d (blue lobe)	27	15	405	55	8×10^3	63

NOTE. — The physical parameters of all these outflows have been obtained with an (sub)millimeter interferometer. a). Parameters obtained from this work. The dynamical age is obtained from Zapata et al. (2009). b). Parameters obtained from this work. The dynamical age is obtained from Zapata et al. (2013a). c). Parameters obtained from Fernández-López et al. (2013). d). Parameters obtained from Qiu et al. (2012). e). Parameters obtained from this work. The dynamical age is obtained from Palau et al. (2006). f). Parameters obtained from Zapata et al. (2015).

radial velocities extracted from the data cube. The filaments do not have clear H_2 counterparts, probably due to the high extinction associated with the extended molecular ridge located in this region, see Zapata et al. (2011). In the lower panel of this Figure, we have computed the PVD of these filaments. This image reveals that these two filaments have in fact different inclination angles with respect to the plane of sky. There is also a good correspondence between the PVD and the position of the CO condensations as in the case of the HH 211 flow. The CO gas kinematics of both filaments show the well defined Hubble laws first reported in Zapata et al. (2009, 2013a). Both filaments point to a common origin. This origin is coincident within the errors with the position from which according to proper motion measurements the radio and infrared sources BN, I, and n were ejected some 500 years ago (Rodríguez et al. 2005; Gómez et al. 2005, 2008). Close to the systemic velocity of the cloud in Orion at about $+9.0 \text{ km s}^{-1}$ and origin of the explosive flow is found the molecular expanding bubble-like outflow reported in Zapata et al. (2011).

Finally, in Figure 4, in the upper panel, we show the image obtained by Zapata et al. (2013a) of the explosive outflow in DR21, and a zoom into a southern region where a bright and isolated filament is discerned. From this region we have selected this filament for our study. The P.A. of the filament is 215° , and we have called DF1. This filament DF1 like the ones we show above for Orion KL is also absent of a H_2 counterpart probably because of high extinction. In the lower panel of this Figure, we have computed the PVD of this filament. The CO gas kinematics of DF1 filament reveals the well defined Hubble law first reported in Zapata et al. (2013a), and also present in the filaments of Orion KL. A similar expanding bubble-like structure seems evident in this PVD. This structure is similar to that mapped in Orion KL region and a detailed analysis of this bubble-like outflow in DR21 will be presented in a future paper.

4. DISCUSSION: EXPLOSIVE VS. PROTOSTELLAR

From an observational point of view the most striking difference between the two types of outflows lies in the different numbers of well-defined, coherent components that make up their structures. As first revealed by SMA interferometric studies of Orion KL (Zapata et al. 2009) and later by ALMA observations (Bally 2016; Bally et al. 2017), an explosive out-

flow essentially consists of dozens to hundreds of individual filaments that extend far in space, show well defined Hubble-like velocity increase with distance, point towards a common center of origin and, taken together, emit the bulk of CO radiation beyond near-ambient frequencies. In contrast, bipolar outflows mostly present one such organized structure only, namely the collimated jet that mobilizes the otherwise chaotic, and incoherent outflow material. This basic difference causes a number of important distinctions between the two classes of outflow, as discussed below.

4.1. Spatial distributions

The protostellar molecular outflows are bipolar in nature, and their spatial distributions of the red- resp. blueshifted components tend to be maximally separated. The bipolarity of the molecular protostellar outflows comes from the fact that the ejected material from the magnetized disks proceed by the two poles of the protostar and the accretion flows in the equator (Pudritz et al. 2007). This is clearly the case of the protostellar outflows studied here, HH 211 and DG Tau B, see the figures presented in Gueth & Guilloteau (1999); Mitchell et al. (1994). The usually large separation between the red- and blue-shifted components in the flows is due mainly to very low probability of having a bipolar outflow perpendicular to the plane of the sky. However, there is an excellent case where an outflow located perpendicular to the plane of the sky has been reported, namely G331.512–0.103 (Merello et al. 2013). This bipolar outflow shows self-absorption features at high velocities, its blueshifted and redshifted sides are overlapped, and has very broad line wings (about 100 km s^{-1}).

However, none of these geometrical effects seem to be the case for the explosive outflows where their spatial distributions of the red- resp. blueshifted components tend to be maximally overlapping. This effect makes the explosive outflows to give the impression that they are located perpendicular to the plane of the sky, and probably driven by wide-angle or precessing outflows from a single massive protostar. Early single dish CO images of the DR 21 and Orion KL showed this observational effect, see Figure 10 of Schneider et al. (2010), and Figure 3a of Rodríguez-Franco et al. (1999). However, SMA interferometric observations revealed that this kind of flows are composed of dozens of collimated molecular fil-

aments with different radial velocities and orientations that points to a single velocity and position center, see Zapata et al. (2009, 2013a). Thus, they are mostly isotropic in all orientations (Figures 3 and 4). See the recent ALMA images made by Bally (2016); Bally et al. (2017) toward the Orion KL explosive outflow. Single dish CO observations could not resolve such collimated filaments, and it was easy to misinterpret the outflow nature. Even though H₂ images from the Orion KL and DR 21 outflows have revealed a northeast/southwest and northwest/southeast bipolar morphology, respectively, see Figures 3 and 4, the flows are indeed nearly isotropic in the sky as revealed in the CO interferometric maps. This apparent bipolarity, noted in the H₂ images, could be explained as due to the high extinction of the dusty filaments crossing the outflows.

As mention earlier, the explosive flows are made of multiple narrow straight filament-like ejections at very different angles, while the classical protostellar outflows show only ejections in a narrow angle window (a central collimated molecular jet, see Figure 1 for instance), surrounded by the characteristic molecular lobes. Such narrow straight filament-like ejections are not bipolar as the classical protostellar outflows. The blue- and red-shifted filament-like ejections are located in a nearly isotropic distribution (see Figure 3 and 4).

4.2. Kinematics

There are marked and striking differences between the PVDs from the protostellar outflows and from the systems of molecular filaments within the explosive flows, see Figures 1, 2, 3, and 4. But the most important kinematical difference is the well defined Hubble flow-like increase of velocity with distance from the origin in the explosive flows versus the non-organized CO velocity fields in protostellar objects. We noted that the PVDs from the protostellar flows sometimes even reveal an anti-Hubble law, where material far from its exciting source shows low radial velocities (Figures 1, and 2), and that this is likely caused because the material far from the outflows is suffering deceleration by the interaction with the surrounding cloud. This seems not to be the case in the explosive filaments, see Figure 3, and 4. But, maybe, some older and fainter explosive filaments could reveal some interactions with its parental cloud using more sensitive observations. For the case of the HH 211 flow, its PVD shown in Figure 1, reveals that part of the outflow appears to have a Hubble velocity law (it is in somehow traced by a pink line in this figure, and is material associated mostly with the molecular jet), probably generated by an internal working surface formed by a temporal variation in the jet velocity and observed in many other HH objects in the optical (Raga et al. 1990; Raga & Cabrit 1993) and submillimeter regimens (Lee et al. 2015).

We note that even when this part of the flow (the collimated jet) appears to have a Hubble-law kinematics, it seems not to point to its exciting source. But, we stress that these two points are not entirely clear, as many other structures with different radial velocities are also overlapping with the collimated jet.

Even when the outflow might seem to have an explosive morphology as in the case of Cepheus A HW2 (Zapata et al. 2013b), its kinematics revealed that this is not the case. The PVDs shown in Figure 8 of Zapata et al. (2013b) exhibit non-organized CO velocity fields, which are more like the ones displayed by the protostellar outflows. Its explosive-like morphology is probably occasioned by a precessing flow

(Cunningham et al. 2009; Zapata et al. 2013b).

A second difference is the kinematic structure of the gas in the protostellar outflows. Both protostellar outflows (DG Tau B and HH 211) reveal “open-fan” structures in their gas kinematics (see the PVD in Figures 1, and 2). These “open-fan” structures are composed of multiple bow-shocks at different positions and radial velocities, see the PVD in Figure 1, where we have marked the bow-shocks. The bow-shocks have a large spread of radial velocities with a more or less constant position (Figure 1), and a curved morphology. These bow-shocks are formed by the interaction of the neutral jet ejected from the young star with the dense molecular gas. These structures are not observed in the PVDs of explosive outflows, see Figures 1, and 2, probably because these flows are not driven by a stellar wind interacting for a long time with the cloud. However, we note that at least for the case of the outflow in DR21, there are some features that could also be bow-shocks within the filaments (see Figure 4). This physical characteristic is in agreement with the explosive filaments being dense fragments of expelled material traveling into the ISM.

4.3. Energetics

In Table 1, it is estimated the mass, momentum, energy, and mechanical luminosity of the explosive filaments versus low-mass protostellar outflows. We want to remark that we are comparing the energetics of the molecular filaments, not the whole explosive outflow, with the protostellar outflows. For comparison we have also included the energetics of some massive molecular outflows, see Table 1. We have estimated the presented physical values in Table 1 from the equations provided in Zapata et al. (2015). However, for the protostellar massive outflows: IRAS 18162–2048-NW, and IRAS 18360–0537, we obtained them from Fernández-López et al. (2013); Qiu et al. (2012). We do not find any marked difference between the values obtained for the massive protostellar outflow IRAS 18162–2048-NW, and the explosive filaments. But, if we take the protostellar outflow IRAS 18360–0537, this clearly shows quite high values for the mass and momentum, compared with the explosive filaments. The outflow IRAS 18162–2048-NW is energized from a B-type pre-main sequence star, while IRAS 18360–0537 is likely energized by O-type young star, and probably this explains the difference in the energetics. For the case of the low-mass flows, there are huge differences in mass, momentum and energy compared with the explosive filaments, suggesting again a different nature. We note that all the physical parameters estimated here are from interferometric observations using the SMA.

4.4. Conclusions

We have analyzed sensitive CO line SMA archival observations from the classical protostellar outflows DG TAU B and HH 211 and the explosive ones: Orion KL and DR 21. Our conclusions are as follows.

1. The CO morphology of both kinds of flows shows largely different spatial distributions of the red- and blue-shifted components: maximally separated in protostellar, and largely overlapping in explosive outflows. The explosive outflows consist of numerous narrow straight filament-like ejections with different orientations, while the classical protostellar outflows show ejections in a very narrow angle window, *i.e.* the colli-

mated jet. The filament-like ejections are not bipolar as in the case of the protostellar flows.

2. An in-depth study of the kinematics of the CO gas of the flows, reveals in the explosive outflows a very well-defined Hubble flow-like increase of velocity with distance from the origin in contrast to the non-organized CO velocity field in protostellar objects. In the protostellar outflows we commonly find well defined bow-shocks (better traced in the case of HH 211 outflow) with different velocity gradients at random positions, likely produced by the interaction of the primary jet with the molecular cloud. In the case of the explosive filaments, we found some bow-shocks-like structures (better observed in the DR21 outflow), but this needs more high angular, sensitive observations to study their nature.
3. We report huge differences in mass, momentum and

energy between the explosive filaments, and low-mass protostellar flows. However, we noted that such physical parameters for the filaments in the explosive outflows agree well with those of a B spectral-type protostar molecular outflow.

This study thus provides new ways to distinguish between the two types of flows. With the discovery of more explosive outflows we will unravel their nature and the physical processes that generate this phenomenon.

LAZ, LFR, AP, and LL acknowledge the financial support from DGAPA, UNAM, and CONACyT, México. We are very thankful for the thoughtful suggestions of the anonymous referee that helped to improve our manuscript.

Facilities: The Submillimeter Array.

REFERENCES

- Allen, D. A., & Burton, M. G. 1993, *Nature*, 363, 54
- Arce, H. G., Shepherd, D., Gueth, F., et al. 2007, *Protostars and Planets V*, 245
- Bally, J., Ginsburg, A., Silvia, D., & Youngblood, A. 2015, *A&A*, 579, A130
- Bally, J., Cunningham, N. J., Moeckel, N., et al. 2011, *ApJ*, 727, 113
- Bally, J., & Zinnecker, H. 2005, *AJ*, 129, 2281
- Bally, J. 2016, *ARA&A*, 54, 491
- Bally, J., Ginsburg, A., Arce, H., et al. 2017, arXiv:1701.01906
- Beuther, H., Schilke, P., Gueth, F., et al. 2002, *A&A*, 387, 931
- Cunningham, N. J., Moeckel, N., & Bally, J. 2009, *ApJ*, 692, 943
- Davis, C. J., Kumar, M. S. N., Sandell, G., et al. 2007, *MNRAS*, 374, 29
- Doi, T., O'Dell, C. R., & Hartigan, P. 2002, *AJ*, 124, 445
- Gómez, L., Rodríguez, L. F., Loinard, L., Lizano, S., Poveda, A., & Allen, C. 2005, *ApJ*, 635, 1166
- Gómez, L., Rodríguez, L. F., Loinard, L., Lizano, S., Allen, C., Poveda, A., & Menten, K. M. 2008, *ApJ*, 685, 333
- Gooch, R. 1996, *Astronomical Data Analysis Software and Systems V*, 101, 80
- Gueth, F., & Guilloteau, S. 1999, *A&A*, 343, 571
- Frank, A., Ray, T. P., Cabrit, S., et al. 2014, *Protostars and Planets VI*, 451
- Fernández-López, M., Girart, J. M., Curiel, S., et al. 2013, *ApJ*, 778, 72
- Froebrich, D. 2005, *ApJS*, 156, 169
- Harvey, P. M., Campbell, M. F., & Hoffmann, W. F. 1977, *ApJ*, 211, 786
- Hirano, N., Liu, S.-Y., Shang, H., et al. 2006, *ApJ*, 636, L141
- Jones, B. F., & Cohen, M. 1986, *ApJ*, 311, L23
- Kleinmann, D. E., & Low, F. J. 1967, *ApJ*, 149, L1
- Klaassen, P. D., Johnston, K. G., Leurini, S., & Zapata, L. A. 2015, *A&A*, 575, A54
- Kwan, J., & Scoville, N. 1976, *ApJ*, 210, L39
- Lee, C.-F., Hirano, N., Zhang, Q., et al. 2015, *ApJ*, 805, 186
- Leurini, S., Codella, C., Zapata, L. A., et al. 2009, *A&A*, 507, 1443
- Masson, C. R., & Chernin, L. M. 1993, *ApJ*, 414, 230
- McCaughrean, M. J., Rayner, J. T., & Zinnecker, H. 1994, *ApJ*, 436, L189
- Merello, M., Bronfman, L., Garay, G., et al. 2013, *ApJ*, 774, L7
- Mitchell, G. F., Hasegawa, T. I., Dent, W. R. F., & Matthews, H. E. 1994, *ApJ*, 436, L177
- Mundt, R., & Fried, J. W. 1983, *ApJ*, 274, L83
- O'Dell, C. R., & Henney, W. J. 2008, *AJ*, 136, 1566
- Palau, A., Ho, P. T. P., Zhang, Q., et al. 2006, *ApJ*, 636, L137
- Pudritz, R. E., Ouyed, R., Fendt, C., & Brandenburg, A. 2007, *Protostars and Planets V*, 277
- Plunkett, A. L., Arce, H. G., Mardones, D., et al. 2015, *Nature*, 527, 70
- Qiu, K., Zhang, Q., Wu, J., & Chen, H.-R. 2009, *ApJ*, 696, 66
- Qiu, K., Zhang, Q., Beuther, H., & Fallscheer, C. 2012, *ApJ*, 756, 170
- Raga, A., & Cabrit, S. 1993, *A&A*, 278, 267
- Raga, A. C., Binette, L., Canto, J., & Calvet, N. 1990, *ApJ*, 364, 601
- Rivilla, V. M., Jiménez-Serra, I., Martín-Pintado, J., & Sanz-Forcada, J. 2014, *MNRAS*, 437, 1561
- Rodríguez-Franco, A., Martín-Pintado, J., & Wilson, T. L. 1999, *A&A*, 351, 1103
- Rodríguez, L. F., Zapata, L. A., & Palau, A. 2014, *ApJ*, 790, 80
- Rodríguez, L. F., Poveda, A., Lizano, S., & Allen, C. 2005, *ApJ*, 627, L65
- Rodríguez, L. F., Zapata, L. A., & Ho, P. T. P. 2009, *ApJ*, 692, 162
- Sault, R. J., Teuben, P. J., & Wright, M. C. H. 1995, *Astronomical Data Analysis Software and Systems IV*, 77, 433
- Schneider, N., Csengeri, T., Bontemps, S., et al. 2010, *A&A*, 520, A49
- Tappe, A., Froebrich, J., Martín, S., Yuan, Y., & Lada, C. J. 2012, *ApJ*, 751, 9
- Youngblood, A., Ginsburg, A., & Bally, J. 2016, *AJ*, 151, 173
- Zapata, L. A., Schmid-Burgk, J., Ho, P. T. P., Rodríguez, L. F., & Menten, K. M. 2009, *ApJ*, 704, L45
- Zapata, L. A., Loinard, L., Schmid-Burgk, J., et al. 2011, *ApJ*, 726, L12
- Zapata, L. A., Schmid-Burgk, J., Pérez-Goytia, N., et al. 2013, *ApJ*, 765, L29
- Zapata, L. A., Fernández-López, M., Curiel, S., Patel, N., & Rodríguez, L. F. 2013, arXiv:1305.4084
- Zapata, L. A., Lizano, S., Rodríguez, L. F., et al. 2015, *ApJ*, 798, 131